The International Journal of Advanced Manufacturing Technology (2019) 103:4695–4702
https://doi.org/10.1007/s00170-019-03932-7

ORIGINAL ARTICLE

Geometry and dilution rate analysis and prediction of laser cladding

Wenchao Xi[1] · Boxue Song[1] · Yu Zhao[1] · Tianbiao Yu[1] · Jun Wang[1]

Received: 7 January 2019 / Accepted: 21 May 2019 / Published online: 6 June 2019
© Springer-Verlag London Ltd., part of Springer Nature 2019

Abstract
Dilution rate is an important factor affecting the properties of laser cladding. However, the exact estimate of dilution rate in direct laser fabrication is still not fully developed. In this study, high-strength and wear-resistant YCF102 alloy powder is used to laser clad on the steel substrate. The area of the cladding layer is replaced by a part of the circle, and the relationship among the deposition angle, the clad width, and the area of the cladding layer is established. The geometry of the fusion zone is replaced by polynomial function of the fourth degree, and the relationship among the thermal tension angle, the clad width, the melting pool depth, and the area of the fusion zone is established. The value of the dilution rate is obtained by the area of the cladding layer and the fusion zone. The correlation coefficient of the area of cladding layer, the area of the fusion zone, and the dilution rate is also obtained. The estimate results coincident with the measurement results very well. The proposed theoretical model offers a basis for estimate of dilution rate in laser cladding.

Keywords Dilution rate · Cladding layer · Fusion zone · Theoretical model

1 Introduction

Direct laser fabrication is an advanced process method by which alloy powder is injected into melting pool through coaxial feeding and forms a cladding layer [1], as shown in Fig. 1. The thickness of the cladding layer is between 50 μm and 2 mm. The geometry and properties of the cladding layer are changed with dilution rate [2]. Many studies have indicated that dilution rate increases with laser energy, and the cladding layer of low dilution rate has well microstructure and mechanical properties [3–6].

In order to improve the forming quality of laser cladding, the geometry of cladding layer is researched. For instance, Kannan et al. [7] suggested a mathematical model of processing parameters for the prediction of cladding layer geometry. Ocelik et al. [8] researched the relationships between laser cladding processing parameters and the main geometrical characteristics of Co-based coatings. Liu et al. [9] analyzed the relationships between processing parameters and output responses (powder catchment efficiency, clad height, clad width), and established a quadratic regression model. Lestan et al. [10] researched the relationships between processing parameters and forming quality, and the results show that crack rate is effectively reduced by preheating substrate. Lalas et al. [11] presented a layer geometry model by considering the mass feed rate and the laser scanning velocity. Arrizubieta et al. [12] presented a powder flow control model that the clad height can be controlled. Nabhani et al. [13] proposed a model for the prediction of clad height, clad width, penetration depth, dilution rate, and wetting angle.

The geometry of melting pool is also studied. For instance, Salehi et al. [14] changed the temperature of melting pool by changing processing parameters to control

✉ Tianbiao Yu
neutianbiaoyu2018@gmail.com

Wenchao Xi
toukonheat@gmail.com

Boxue Song
bamboomoon.harold@gmail.com

Yu Zhao
1097451073@qq.com

Jun Wang
363825394@qq.com

[1] School of Mechanical Engineering and Automation, Northeastern University, Shenyang, People's Republic of China

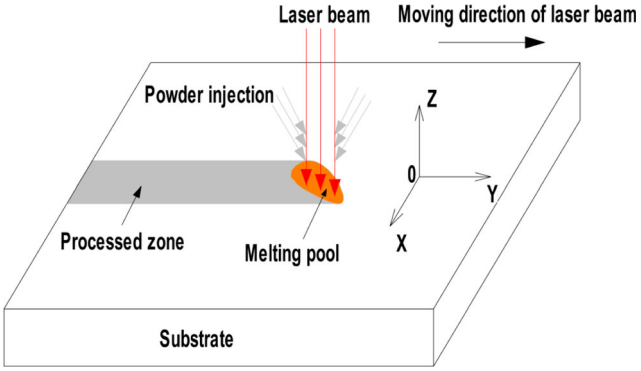

Fig. 1 Schematic diagram of the direct laser fabrication

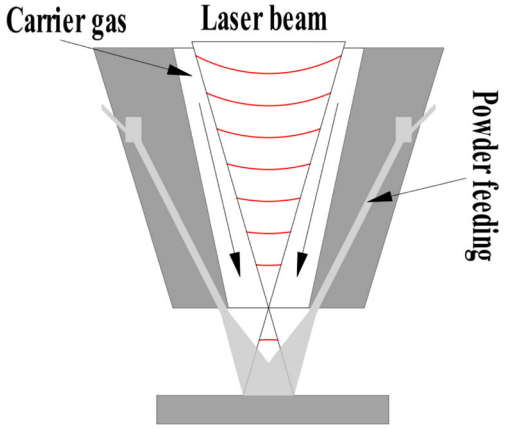

Fig. 2 Schematic diagram of the coaxial nozzle

quality of cladding layer. Partes et al. [15] suggested a melting pool model by considering different powder forms injected into melting pool. Criales et al. [16] researched the relationship processing parameters (laser power, scanning velocity, and powder material's density), and the results show that powder material's density has the greatest effect on the shape of melting pool.

Näkki et al. [17] researched the hot cracking resistance and dilution rate of the Ni-based alloy powder. Kathuria et al. [18] researched microstructure, hardness, and dilution rate of the Co-based layer. Fu et al. [19] proposed a model for calculating the surface temperature distribution based on the mass feed rate and laser scanning velocity. Hofman et al. [20] developed a model that the dilution rate and the cladding layer geometry can be determined. Kattire et al. [21] researched microstructure, residual stress, and micro-hardness of laser cladding on H13 tool steel, and proved the effectiveness of the proposed method. Fathi et al. [22] suggested a model for the prediction of the melting pool depth and the dilution rate.

Accurate estimate of geometry, melting pool, and dilution rate in direct laser fabrication is important in order to improve surface quality and obtain well properties of cladding layer. Despite the numerous research works on estimate of geometry, melting pool, and dilution rate in direct laser fabrication, there are still limitations of the existing estimate model and the measurement results are not in coincidence with the estimate. In this paper, the correlation between processing parameters and dilution rate was researched, and a theoretical model of dilution rate is established. The more accurate estimate of the dilution rate can be obtained by processing parameters.

2 Experimental conditions

In this study, using a 6 degree of freedom KUKA robot, a fiber laser with 500 W power supply and a coaxial nozzle were specially designed according to the laser beam characteristics, as shown in Fig. 2. Due to the limitations of the experimental equipment, laser spot diameter is fixed at 1.1 mm. The powder is flowed by 6 L/min of the carrier gas (Ar) to form a powder flow. The carrier gas (Ar) is used in order to avoid any chemical reaction with the injected powder. The value of 6 L/min is determined by the previous experiment. The carrier gas (Ar) can also take away part of the heat during laser cladding.

In this study, the alloy powder model is YCF102. YCF102 is a high-strength and wear-resistant Fe-based alloy powder, and it is widely used in repairing and laser cladding of machine tool parts. YCF102 alloy powder composition is shown in Table 1. The length of each single laser cladding track is 25 mm. Each single laser cladding track is produced on the same C45E4 steel substrates of 110 × 120 × 10mm^3; C45E4 steel composition is shown in Table 1. In order to avoid the influence of substrate warpage on laser cladding, every two laser cladding tracks are carried out at a distance of 4 mm.

Laser cladding process parameters are measured from the cross sections of the laser cladding tracks (Fig. 3). Cross-sectional characteristics change with power, velocity, and feed mass rate as shown in Figs. 4, 5, 6, 7, 8, 9, 10, 11, and 12. Laser cladding process parameters include clad height (H), clad width (W), melting pool depth (D), deposition angle (θ), thermal tension angle (β), the area of cladding layer (A_1), and fusion zone (A_2) as shown in Fig. 3.

In this study, different scanning velocities V (300, 360, and 420 mm/min), laser powers P (350, 400, and 450 W), and mass feed rates Q_m (0.155, 0.175, and 0.195 g/s) are selected for each signal laser cladding track. The average of the process parameters for two cross sections for each laser cladding track is studied.

3 Results and discussion

As shown in Figs. 4, 5, and 6, laser power and mass feed rate are remaining constant, and clad height and melting pool

Table 1 Chemical composition of the YCF102 alloy powder and C45E4 steel (wt%) (provided by the manufacturer)

Model	C	Si	Mn	Ni	Cr	N	Mo	Nb	Cu	P, S	Fe
YCF102	0.05	0.9	0.4	6.5	15.5	0.22	1.0	0.31	–	–	Bal.
C45E4	0.42–0.5	0.17–0.37	0.5–0.8	≤ 0.25	≤ 0.25	–	–	–	≤ 0.25	≤ 0.045	Bal.

depth are decreased with increasing scanning velocity. This phenomenon is caused by the increase of scanning velocity, the interaction time between laser and material is shortened, and the energy absorption of cladding layer is reduced in unit time. When scanning velocity and mass feed rate are remaining constant, clad width and melting pool depth increase if laser power increases as shown in Figs. 7, 8, and 9. The increase of laser power can shorten the melting time of the alloy powder and increase the interaction time between laser and substrate. As shown in Figs. 10, 11, and 12, laser power and scanning velocity are constant, and clad height increases if mass feed rate increases. Otherwise, melting pool depth decreases with the increase of mass feed rate. This result is due to the increase in the amount of powder entering the melting bath. The alloy powder absorbs more laser energy, resulting the interaction time between laser and substrate shortened.

3.1 Calculation of the cladding layer area

With each single laser cladding track processing parameters change, laser cladding geometry is also changing. According to the geometric characteristics of the cross section, the geometry can always be a part of a circle, where the center can be above or below the workpiece surface as shown in Fig. 13. When the scanning velocity is relatively low or the feed mass rate is relatively high, it will cause the accumulation of the deposited material, and vice versa. In this case, the center of the circle goes above the workpiece surface. The function of this model is to calculate the area by the processing parameters.

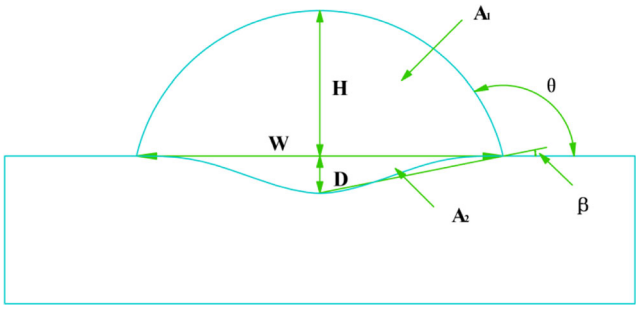

Fig. 3 Schematic diagram of measurement parameters

When the center of the circle goes above or below the workpiece surface, the area is the sum of the circle sector area and the triangle area as shown in Fig. 14, and is given by

$$A_1 = \frac{360°-2\theta}{360°}\pi r^2 + \frac{1}{2}Wy \tag{1}$$

where θ is the deposition angle, r is the radius (in μm), x is the distance from the circle center to the workpiece surface (in μm), given by

$$y = \frac{1}{2}W\cot(\theta) \tag{2}$$

$$r = \frac{W}{2\sin(\theta)} \tag{3}$$

The area of the geometry (A_1) can be represented by the clad width (W) and the deposition angle (θ):

$$A_1 = \frac{1}{4}W^2\left[\left(1-\frac{\theta}{180°}\right)\frac{\pi}{\sin^2(\theta)} + \cot(\theta)\right] \tag{4}$$

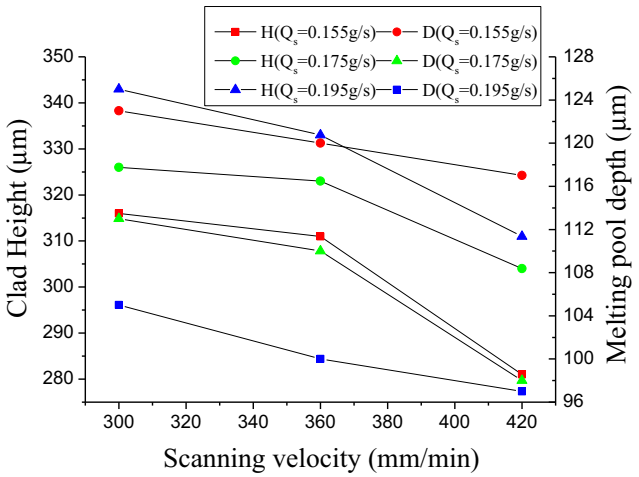

Fig. 4 Effect of scanning velocity on clad height and melting pool depth (P = 350 W)

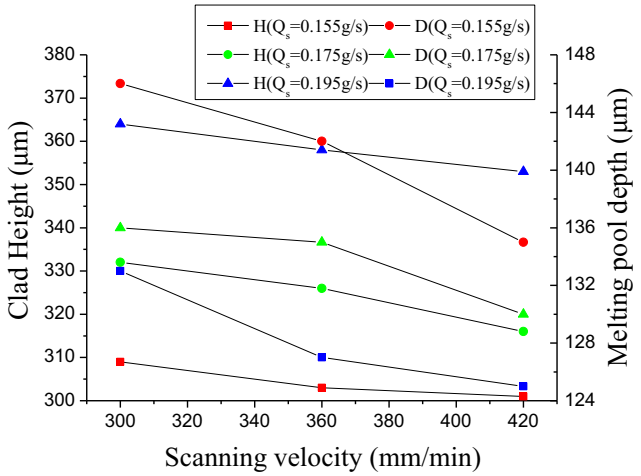

Fig. 5 Effect of scanning velocity on clad height and melting pool depth (P = 400 W)

According to Eq. (4), the area of cladding layer (A_1) can be calculated from the deposition angle (θ) and the clad width (W). When the deposition angle (θ) is the remaining constant, square value of the clad width is proportional to the area of cladding layer (A_1). When the clad width (W) remains constant, the deposition angle (θ) is inversely proportional to the area of the cladding layer (A_1) at the deposition angle greater than 0 degrees and less than 90 degrees. The alloy powder complete melting into the substrate at the deposition angle (θ) is 180 degrees.

3.2 Area calculation of the fusion zone

As shown in Fig. 4, the geometry of the fusion zone is similar to the fourth power function. In this study, it can choose polynomial function of the fourth degree to describe the geometry of the fusion zone, given by

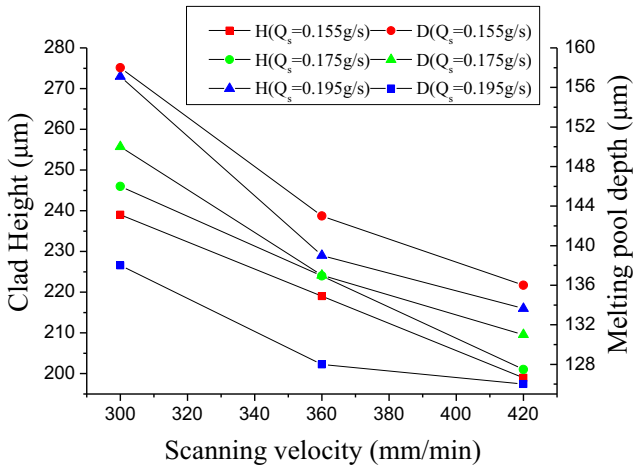

Fig. 6 Effect of scanning velocity on clad height and melting pool depth (P = 450 W)

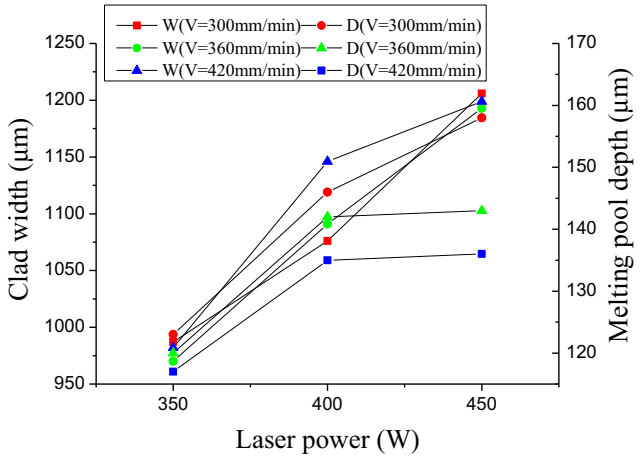

Fig. 7 Effect of laser power on clad width and melting pool depth (Q_m = 0.155 g/s)

$$f(x) = ax^4 + bx^3 + cx^2 + dx + e \tag{5}$$

where a, b, c, d, and e are constants.

According to the geometry of the fusion zone, the following boundary conditions are available:

$$\begin{cases} x = 0, y = -D \\ x = 0, \dfrac{dy}{dx} = 0 \\ x = \dfrac{1}{2}W, y = 0 \\ x = \dfrac{1}{2}W, \dfrac{dy}{dx} = \tan(\beta) \\ x = -\dfrac{1}{2}W, y = 0 \\ x = -\dfrac{1}{2}W, \dfrac{dy}{dx} = -\tan(\beta) \end{cases} \tag{6}$$

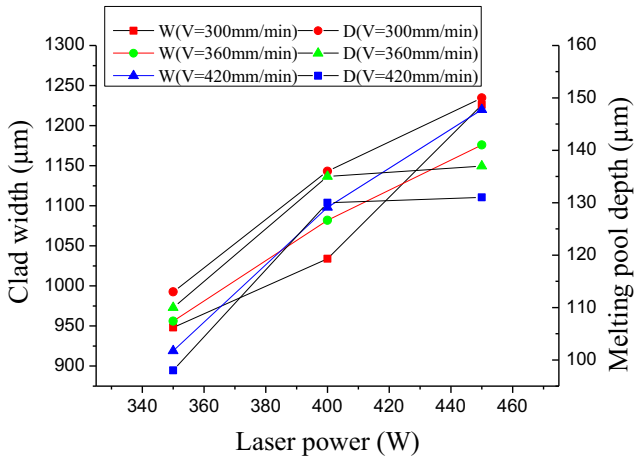

Fig. 8 Effect of laser power on clad width and melting pool depth (Q_m = 0.175 g/s)

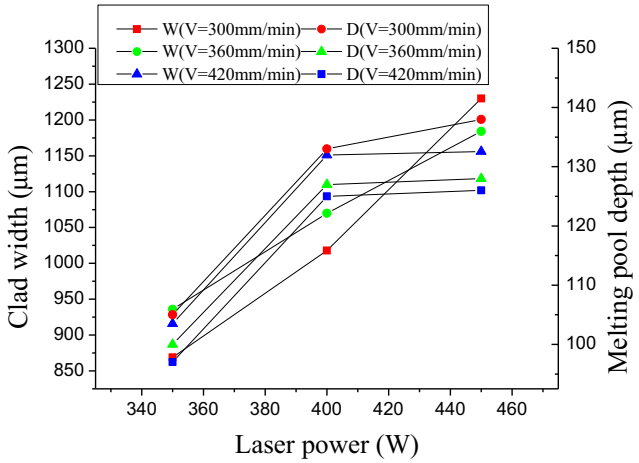

Fig. 9 Effect of laser power on clad width and melting pool depth (Q_m = 0.195 g/s)

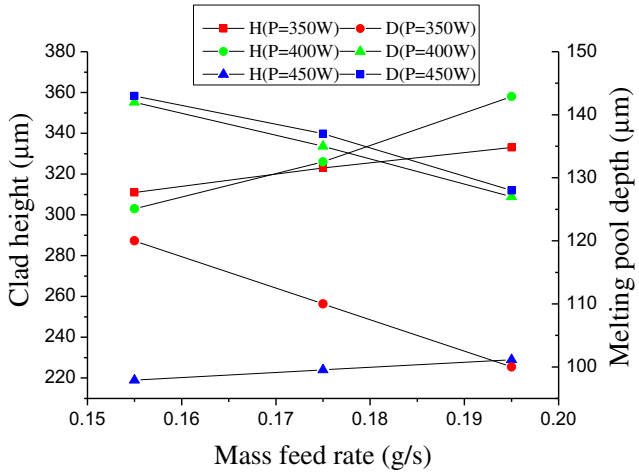

Fig. 11 Effect of mass feed rate on clad height and melting pool depth (V = 360 mm/min)

where β is the thermal tension angle, W is the clad width (in μm), and h is the melting pool depth (in μm).

From Eq. (5) and Eq. (6), the $f(x)$ can be expressed as follows:

$$f(x) = \left(\frac{4W\tan(\beta) - 16D}{W^4}\right)x^4 + \left(\frac{8D - W\tan(\beta)}{W^2}\right)x^2 - D \quad (7)$$

According to Eq. (7), the area of the fusion zone is given by

$$A_2 = \int_{-D}^{0}\left(\frac{4W\tan(\beta) - 16D}{W^4}\right)x^4 + \left(\frac{8D - W\tan(\beta)}{W^2}\right)x^2 - D \quad (8)$$

$$A_2 = \left(\frac{4W\tan(\beta) - 16D}{5W^4}\right)D^5 + \left(\frac{8D - W\tan(\beta)}{3W^2}\right)D^3 - D^2 \quad (9)$$

It is noticed that the area of the fusion zone (A_2) can be calculated by the thermal tension angle (β), the clad width (W), and the melting pool depth (D). When the thermal tension angle (β) and the melting pool depth (D) are remaining constants, the area of the fusion zone (A_2) is inversely proportional to the clad width (W). When the thermal tension angle (β) and the clad width (W) are remaining constants, the area of the fusion zone (A_2) is inversely proportional to the melting pool depth (D). When the clad width (W) and the melting pool depth

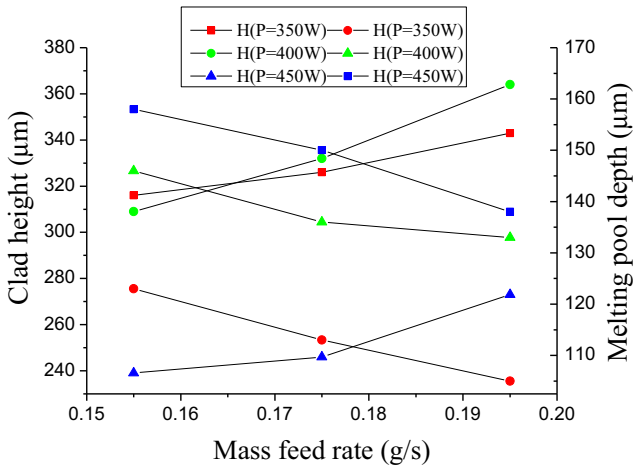

Fig. 10 Effect of mass feed rate on clad height and melting pool depth (V = 300 mm/min)

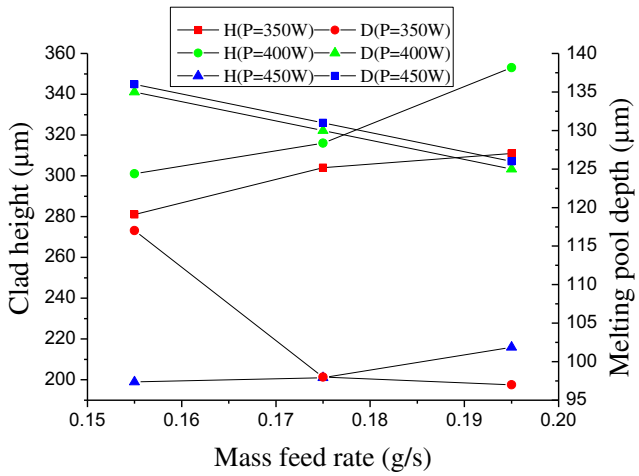

Fig. 12 Effect of mass feed rate on clad height and melting pool depth (V = 420 mm/min)

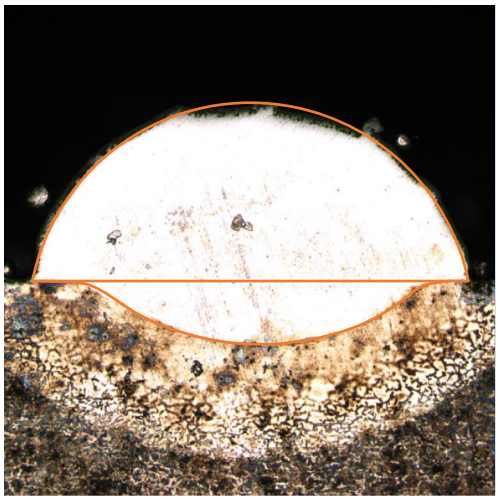

Fig. 13 Geometric characteristics of the cross section

(D) are remaining constants, the area of the fusion zone (A_2) is proportional to the thermal tension angle (β).

3.3 Calculation and measurement of the dilution rate

Dilution rate directly affects the properties of the laser cladding. The amount of the alloy powder diluted in the substrate is increasing if dilution rate is increasing. Increasing the dilution rate directly affects the inherent properties of the laser cladding, and increasing the possibility of cracking and deformation of the laser cladding. However, with a decrease of dilution rate, the area of fusion zone decreased, which led to the decrease of bonding force between cladding layer and substrate.

The formula of dilution rate [23] is given by

$$\lambda = \frac{A_2}{A_1 + A_2} \tag{10}$$

where A_1 is the area of the cladding layer, and A_2 is the area of the fusion zone. According to Eqs. (4), (9), and (10), the dilution rate (λ) can be expressed as follows:

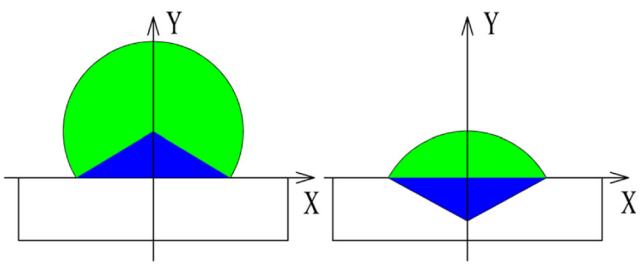

Fig. 14 Schematic diagram of the fan area and the triangle area

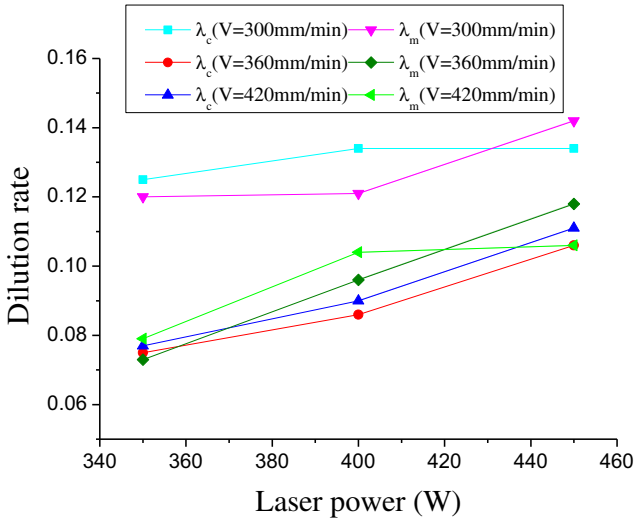

Fig. 15 Effect of laser power on dilution rate (Q_m = 0.155 g/s)

$$\lambda = \frac{\left(\frac{4W\tan(\beta)-16D}{5W^4}\right)D^5 + \left(\frac{8D-W\tan(\beta)}{3W^2}\right)D^3 - D^2}{\frac{1}{4}W^2\left[\left(1-\frac{\theta}{180°}\right)\frac{\pi}{\sin^2(\theta)} + \cot(\theta)\right] + \left(\frac{4W\tan(\beta)-16D}{5W^4}\right)D^5 + \left(\frac{8D-W\tan(\beta)}{3W^2}\right)D^3 - D^2} \tag{11}$$

The area of cladding layer and fusion zone was obtained by a 3D measuring laser microscope, and the dilution rate measurement (λ_m) was obtained by Eq. (10).

In Figs. 15, 16, and 17, λ_c is the calculated value of the dilution rate and λ_m is the measurement value of the dilution rate.

According to Figs. 15, 16, and 17, the dilution rate is increasing if the laser power is increasing, because the increase of laser power can reduce the melting time of the alloy powder and increase the interaction time between alloy powder and substrate.

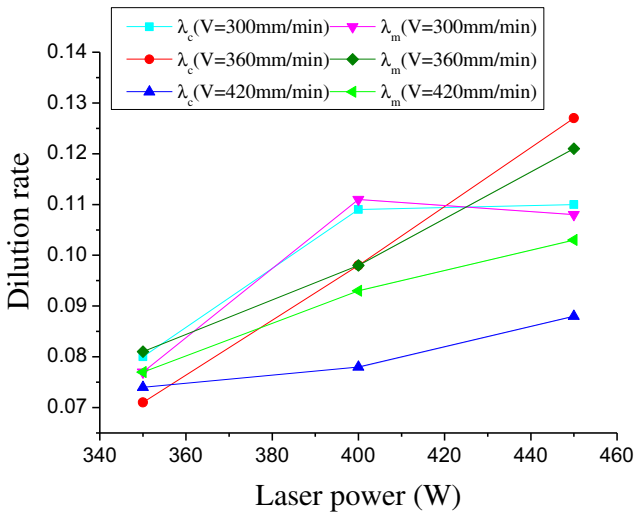

Fig. 16 Effect of laser power on dilution rate (Q_m = 0.175 g/s)

3.4 Residuals and correlation coefficient

The formula of residual (R) is given by

$$R = \lambda_c - \lambda_m \tag{12}$$

It is noticed that the trend of the dilution rate calculated and the dilution rate measurement is the same. As shown in Fig. 18, residual values are randomly distributed in the above or below the line equal to zero, indicating that the fitting of the dilution rate calculated to the dilution rate measurement is satisfactory. The average value of residuals is − 0.003. This results show that the calculated value of the dilution rate (λ_c) is approximate to the measurement value of dilution rate (λ_m), and it is noticed that theoretical model of the dilution rate is reasonable.

In this study, Pearson correlation coefficient is used to calculate the closeness of the calculated value of the dilution rate (λ_c) and the measurement value of the dilution rate (λ_m) relationships. The formula of Pearson correlation coefficient is given by

$$r(\lambda_c, \lambda_m) = \frac{n\sum\lambda_c \cdot \lambda_m - \sum\lambda_c \sum\lambda_m}{\sqrt{n\sum\lambda_c{}^2 - (\sum\lambda_c)^2} \cdot \sqrt{n\sum\lambda_m{}^2 - (\sum\lambda_m)^2}} \tag{13}$$

According to Eq. (13), the correlation coefficient between the calculated value and the measurement value of the dilution rate is 0.92. The correlation coefficient between the calculated value and the measurement value of the area of the geometry is 0.68, and the correlation coefficient between the calculated value and the measurement value of the area of the fusion zone is 0.89. It shows that this method can estimate the dilution rate, but the results of the estimate of the area of the geometry and the fusion zone are not accurate enough.

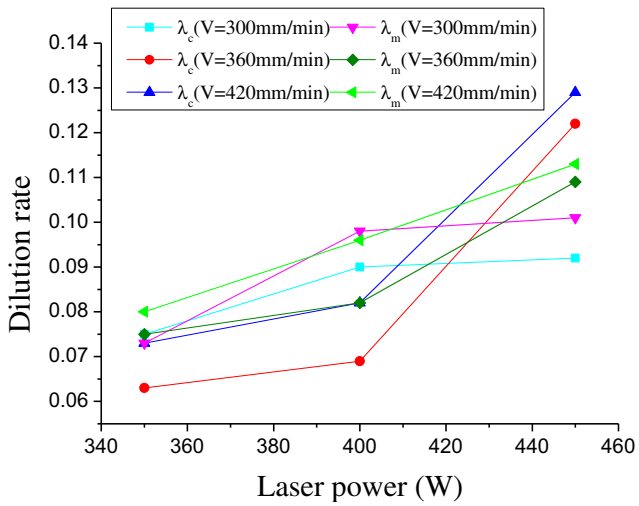

Fig. 17 Effect of laser power on dilution rate (Q_m = 0.195 g/s)

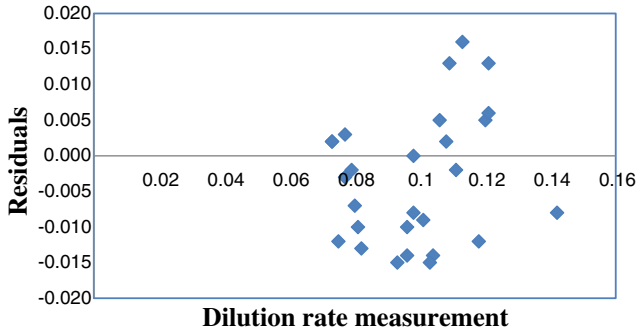

Fig. 18 Residuals of the dilution rate

4 Conclusion

(1) The relationship among the deposition angle, the clad width, and the area of the cladding layer is established, to realize the prediction of cross-section area of cladding layer.

(2) The relationship among the thermal tension angle, the clad width, the melting pool depth, and the area of the fusion zone is established, to realize the prediction of fusion zone area.

(3) The theoretical model of the dilution rate is established, and the rationality of this model is verified by residual and correlation coefficient. The correlation analysis shows a high correlation between measured and estimated dilution rates.

Funding information This work was financially supported by Ministry of Industry and Information Technology (201675514) and Key Laboratory of Shenyang (15153100).

References

1. El Cheikh H, Courant B, Branchu S, Hascoët J, Guillén R (2012) Analysis and prediction of single laser tracks geometrical characteristics in coaxial laser cladding process. Opt Lasers Eng 50(3): 413–422. https://doi.org/10.1016/j.optlaseng.2011.10.014
2. Song L, Bagavath-Singh V, Dutta B, Mazumder J (2012) Control of melt pool temperature and deposition height during direct metal deposition process. Int J Adv Manuf Technol 58(1–4):247–256. https://doi.org/10.1007/s00170-011-3395-2
3. Huang Y (2011) Characterization of dilution action in laser-induction hybrid cladding. Opt Laser Technol 43(5):965–973. https://doi.org/10.1016/j.optlastec.2010.12.005
4. Marzban J, Ghaseminejad P, Ahmadzadeh MH, Teimouri R (2015) Experimental investigation and statistical optimization of laser surface cladding parameters. Int J Adv Manuf Technol 76(5–8):1163–1172. https://doi.org/10.1007/s00170-014-6338-x
5. Candel JJ, Amigó V, Ramos JA, Busquets D (2010) Sliding wear resistance of TiC p reinforced titanium composite coating produced by laser cladding. Surf Coat Technol 204(20):3161–3166. https://doi.org/10.1016/j.surfcoat.2010.02.070

6. Liu H, Hu Z, Qin X, Wang Y, Zhang J, Huang S (2017) Parameter optimization and experimental study of the sprocket repairing using laser cladding. Int J Adv Manuf Technol 91(9–12):3967–3975. https://doi.org/10.1007/s00170-017-0066-y
7. Kannan T, Yoganandh J (2010) Effect of process parameters on clad bead geometry and its shape relationships of stainless steel claddings deposited by GMAW. Int J Adv Manuf Technol 47(9–12): 1083–1095. https://doi.org/10.1007/s00170-009-2226-1
8. Ocelík V, De Oliveira U, De Boer M, De Hosson J (2007) Thick Co-based coating on cast iron by side laser cladding: analysis of processing conditions and coating properties. Surf Coat Technol 201(12):5875–5883. https://doi.org/10.1016/j.surfcoat.2006.10.044
9. Liu S, Kovacevic R (2014) Statistical analysis and optimization of processing parameters in high-power direct diode laser cladding. Int J Adv Manuf Technol 74(5–8):867–878. https://doi.org/10.1007/s00170-014-6041-y
10. Lestan Z, Milfelner M, Balic J, Brezocnik M, Karabegovic I (2013) Laser deposition of Metco 15E, Colmony 88 and VIM CRU 20 powders on cast iron and low carbon steel. Int J Adv Manuf Technol 66(9–12):2023–2028. https://doi.org/10.1007/s00170-012-4478-4
11. Lalas C, Tsirbas K, Salonitis K, Chryssolouris G (2007) An analytical model of the laser clad geometry. Int J Adv Manuf Technol 32(1):34–41. https://doi.org/10.1007/s00170-005-0318-0
12. Arrizubieta JI, Martínez S, Lamikiz A, Ukar E, Arntz K, Klocke F (2017) Instantaneous powder flux regulation system for laser metal deposition. J Manuf Process 29:242–251. https://doi.org/10.1016/j.jmapro.2017.07.018
13. Nabhani M, Razavi RS, Barekat M (2018) An empirical-statistical model for laser cladding of Ti-6Al-4V powder on Ti-6Al-4V substrate. Opt Laser Technol 100:265–271. https://doi.org/10.1016/j.optlastec.2017.10.015
14. Salehi D, Brandt M (2006) Melt pool temperature control using LabVIEW in Nd: YAG laser blown powder cladding process. Int J Adv Manuf Technol 29(3–4):273–278. https://doi.org/10.1007/s00170-005-2514-3
15. Partes K (2009) Analytical model of the catchment efficiency in high speed laser cladding. Surf Coat Technol 204(3):366–371. https://doi.org/10.1016/j.surfcoat.2009.07.041
16. Criales LE, Arısoy YM, Özel T (2016) Sensitivity analysis of material and process parameters in finite element modeling of selective laser melting of Inconel 625. Int J Adv Manuf Technol 86(9–12): 2653–2666. https://doi.org/10.1007/s00170-015-8329-y
17. Näkki J, Tuominen J, Vuoristo P (2017) Effect of minor elements on solidification cracking and dilution of alloy 625 powders in laser cladding. J Laser Appl 29(1):012014. https://doi.org/10.2351/1.4973673
18. Kathuria YP (2000) Some aspects of laser surface cladding in the turbine industry. Surf Coat Technol 132(2):262–269. https://doi.org/10.1016/S0257-8972(00)00735-0
19. Fu Y, Loredo A, Martin B, Vannes AB (2002) A theoretical model for laser and powder particles interaction during laser cladding. J Mater Process Technol 128(1):106–112. https://doi.org/10.1016/S0924-0136(02)00433-8
20. Hofman JT, De Lange DF, Pathiraj B, Meijer J (2011) FEM modeling and experimental verification for dilution control in laser cladding. J Mater Process Technol 211(2):187–196. https://doi.org/10.1016/j.jmatprotec.2010.09.007
21. Kattire P, Paul S, Singh R, Yan W (2015) Experimental characterization of laser cladding of CPM 9V on H13 tool steel for die repair applications. J Manuf Process 20:492–499. https://doi.org/10.1016/j.jmapro.2015.06.018
22. Fathi A, Toyserkani E, Khajepour A, Durali M (2006) Prediction of melt pool depth and dilution in laser powder deposition. J Phys D Appl Phys 39(12):2613–2623. https://doi.org/10.1088/0022-3727/39/12/022
23. Lian G, Yao M, Zhang Y, Chen C (2018) Analysis and prediction on geometric characteristics of multi-track overlapping laser cladding. Int J Adv Manuf Technol 97(5–8):2397–2407. https://doi.org/10.1007/s00170-018-2107-6

Publisher's note Springer Nature remains neutral with regard to jurisdictional claims in published maps and institutional affiliations.